

GGPS1 Mutations Cause Muscular Dystrophy/Hearing Loss/Ovarian Insufficiency Syndrome

A. Reghan Foley, MD ¹, Yaqun Zou, MD,¹ James E. Dunford, PhD,²
Jachinta Rooney, PhD,¹ Goutam Chandra, PhD,³ Hui Xiong, MD,⁴ Volker Straub, MD,⁵
Thomas Voit, MD,⁶ Norma Romero, MD, PhD,⁷ Sandra Donkervoort, MS, CGC,¹
Ying Hu, MS,¹ Thomas Markello, MD, PhD,⁸ Adam Horn, PhD,³ Leila Qebibo, MD,⁹
Jahannaz Dastgir, DO,^{1,10} Katherine Meilleur, PhD,^{1,11} Richard S. Finkel, MD,^{12,13}
Yanbin Fan, MD,⁴ Kamel Mamchaoui, PhD,⁷ Stephanie Duguez, PhD,^{7,14}
Isabelle Nelson, PhD,⁷ Jocelyn Laporte, PhD,¹⁵ Mariarita Santi, MD,¹⁶
Edoardo Malfatti, MD, PhD,^{7,17,18} Thierry Maisonobe, MD,⁷ Philippe Touraine, MD, PhD,¹⁹
Michio Hirano, MD,²⁰ Imelda Hughes, MD,²¹ Kate Bushby, MD,⁵
Udo Oppermann, PhD,^{2,22,23} Johann Böhm, PhD ¹⁵, Jyoti K. Jaiswal, PhD ^{3,24}
Tanya Stojkovic, MD,²⁵ and Carsten G. Bönnemann, MD¹

View this article online at wileyonlinelibrary.com. DOI: 10.1002/ana.25772

Received Feb 5, 2020, and in revised form May 5, 2020. Accepted for publication May 6, 2020.

Address correspondence to Dr Bönnemann, Neuromuscular and Neurogenetic Disorders of Childhood Section Senior Investigator, Neurogenetics Branch National Institute of Neurological Disorders and Stroke/NIH Porter Neuroscience Research Center 35 Convent Drive, Bldg 35, Room 2A-116 Bethesda, MD 20892-3705. E-mail: carsten.bonnemann@nih.gov

From the ¹Neuromuscular and Neurogenetic Disorders of Childhood Section, National Institute of Neurological Disorders and Stroke, National Institutes of Health, Bethesda, Maryland; ²Botnar Research Centre, National Institute for Health Research Biomedical Research Centre Oxford, University of Oxford, Oxford, United Kingdom; ³Children's National Health System, Center for Genetic Medicine Research, Washington, District of Columbia; ⁴Department of Pediatrics, Peking University First Hospital, Beijing, China; ⁵Institute of Genetic Medicine, International Centre for Life, Newcastle upon Tyne, United Kingdom; ⁶Great Ormond Street Hospital Biomedical Research Centre, Great Ormond Street Institute of Child Health, London, United Kingdom; ⁷Sorbonne University, Institute of Myology and Public Hospital Network of Paris, Paris, France; ⁸National Institutes of Health Undiagnosed Diseases Program, National Human Genome Research Institute, Bethesda, Maryland; ⁹Unit of Medical Genetics and Oncogenetics, University Hospital, Fes, Morocco; ¹⁰Department of Pediatric Neurology, Goryeb Children's Hospital, Morristown, New Jersey; ¹¹Biogen, Cambridge, Massachusetts; ¹²Division of Neurology, Children's Hospital of Philadelphia, Philadelphia, Pennsylvania; ¹³Division of Neurology, Department of Pediatrics, Nemours Children's Hospital, Orlando, Florida; ¹⁴School of Biomedical Sciences, Ulster University, Derry, United Kingdom; ¹⁵Institute of Genetics and Molecular and Cellular Biology, Strasbourg University, Illkirch, France; ¹⁶Department of Pathology and Laboratory Medicine, Children's Hospital of Philadelphia, Philadelphia, Pennsylvania; ¹⁷National Institute of Health and Medical Research U1179, Versailles Saint-Quentin-en-Yvelines University, Versailles, France; ¹⁸Raymond Poincaré University Hospital, Garches, France; ¹⁹Department of Endocrinology and Reproductive Medicine, Faculty of Medicine, Sorbonne University, Pitié-Salpêtrière Hospital, Public Hospital Network of Paris, Reference Center for Rare Endocrine Diseases of Growth and Development, Paris, France; ²⁰Department of Neurology, H. Houston Merritt Neuromuscular Research Center, Columbia University Medical Center, New York, New York; ²¹Department of Paediatric Neurology, Royal Manchester Children's Hospital, Manchester, United Kingdom; ²²Structural Genomics Consortium, University of Oxford, Oxford, United Kingdom; ²³Freiburg Institute of Advanced Studies, University of Freiburg, Freiburg, Germany; ²⁴Department of Genomics and Precision Medicine, George Washington University School of Medicine and Health Sciences, Washington, District of Columbia; and ²⁵Faculty of Medicine, Sorbonne University, Pitié-Salpêtrière Hospital, Public Hospital Network of Paris, Reference Center for Neuromuscular Diseases North/East/Ile de France, Paris, France

Objective: A hitherto undescribed phenotype of early onset muscular dystrophy associated with sensorineural hearing loss and primary ovarian insufficiency was initially identified in 2 siblings and in subsequent patients with a similar constellation of findings. The goal of this study was to understand the genetic and molecular etiology of this condition.

Methods: We applied whole exome sequencing (WES) superimposed on shared haplotype regions to identify the initial biallelic variants in *GGPS1* followed by *GGPS1* Sanger sequencing or WES in 5 additional families with the same phenotype. Molecular modeling, biochemical analysis, laser membrane injury assay, and the generation of a Y259C knock-in mouse were done.

Results: A total of 11 patients in 6 families carrying 5 different biallelic mutations in specific domains of *GGPS1* were identified. *GGPS1* encodes geranylgeranyl diphosphate synthase in the mevalonate/isoprenoid pathway, which catalyzes the synthesis of geranylgeranyl diphosphate, the lipid precursor of geranylgeranylated proteins including small guanosine triphosphatases. All but one patient presented with congenital sensorineural hearing loss and proximal weakness, and all postpubertal females had primary ovarian insufficiency. Muscle histology was dystrophic, with ultrastructural evidence of autophagic material and large mitochondria in the most severe cases. There was delayed membrane healing after laser injury in patient-derived myogenic cells, and a knock-in mouse of one of the mutations (Y259C) resulted in prenatal lethality.

Interpretation: The identification of specific *GGPS1* mutations defines the cause of a unique form of muscular dystrophy with hearing loss and ovarian insufficiency and points to a novel pathway for this clinical constellation.

ANN NEUROL 2020;00:1–15

The muscular dystrophies are degenerative disorders of muscle characterized by evidence of degeneration and regeneration on muscle histology and are typically associated with elevated creatine kinase (CK) as a measure of ongoing muscle fiber breakdown. Mechanisms and pathways that underlie muscular dystrophies are diverse and include extracellular, membrane-centered, sarcomeric, nuclear, and mitochondrial as well as metabolic mechanisms.¹ In the dystrophies that involve membrane stability or repair, serum CK values are typically elevated as a sign of membrane leakage. Congenital sensorineural hearing loss rarely manifests in association with muscular dystrophy but has been reported in early onset facioscapulohumeral muscular dystrophy.² Perrault syndrome, caused by mutations in various mitochondrial and peroxisomal genes, clinically manifests with sensorineural hearing loss and primary ovarian insufficiency but without muscle involvement³; a combination of muscular dystrophy with primary ovarian insufficiency has not been recognized yet.

The mevalonate pathway is a central metabolic shuttle for the synthesis of specialized lipids. Mevalonic acid is formed from acetyl-CoA via HMG-CoA and then further metabolized to C14-isopentenyl pyrophosphate (IPP), which is subsequently converted to farnesyl-pyrophosphate (FPP), which serves as a precursor for the squalene cholesterol pathway as well as for protein prenylation,⁴ which includes farnesylation as well as geranylgeranylation. Prenylation adds a hydrophobic lipid tail to proteins, allowing for anchorage to membranes for precise subcellular localization, typically within membranes. Prenylation is of particular relevance for small guanosine triphosphatases (GTPases), including those of the Rho and Ras/Rab families. For geranylgeranylation, FPP has to be converted to geranylgeranyl-pyrophosphate (GGPP), by geranylgeranyl diphosphate synthetase (GGPPS; EC:2.5.1.29), encoded by *GGPS1*. GGPP will then be

transferred by 2 types of geranylgeranyl transferase (GGTase I or GGTase II) onto the recipient proteins. Whereas some of the small GTPases are only farnesylated or can alternatively be farnesylated or geranylgeranylated, some are exclusively dependent on geranylgeranylation for their prenylation. More than 100 human proteins are predicted to be targets for geranylgeranylation; among them are prominently small GTPases of the Rab family, many of which are involved in tagging membranes of endoplasmic reticulum, Golgi, endosome Golgi, lysosomes, autophagic vesicles, cell membranes, and mitochondria, as well as of the Rho/Rac family, involved in cytoskeletal actin dynamics among other roles.^{5–7} Other functions of GGPP include negative feedback regulation of the mevalonate pathway by inducing HMG-CoA reductase misfolding, ubiquitination, and degradation.⁸ Some GGPP may also enter into ubiquinone, coenzyme Q, and squalene synthesis; however, FPP is the major source for this biosynthetic branch. It is also possible that there are additional, not yet explored functions and uses for GGPP in the cell.⁹ Although thus far there has been no human monogenic disease linked to mutations in *GGPS1*, it has been identified as a risk factor for atypical femoral bone fractures in females exposed to bisphosphonates.^{10–12}

Here, we report specific mutations in the gene *GGPS1* coding for the enzyme geranylgeranyl pyrophosphate synthetase in 11 patients from 6 families, causing a highly distinctive syndrome of early onset muscular dystrophy combined with congenital sensorineural hearing loss and primary ovarian insufficiency in females. The mutations do not abolish enzymatic activity of this essential enzyme, but with a highly distinctive genotype/phenotype correlation define the mevalonate pathway as essential for muscle, hearing, and endocrine functions.

Subjects and Methods

Patient Recruitment and Sample Collection

Patients P1, P2, and P7 were consented and enrolled in the study approved by the institutional review board (IRB) of the National Institute of Neurological Disorders and Stroke, National Institutes of Health (NIH; 12-N-0095). Patient P3 was enrolled via the Institute of Genetic Medicine, International Centre for Life's Biobank (National Research Ethics Service Committee North East–Newcastle & North Tyneside; Research Ethics Committee [REC] reference: 08/H0906/28 + 5). Patients P4–P6 and patient P8 were enrolled via the Institute of Myology and Public Hospital Network of Paris, Pitié-Salpêtrière Hospital Group (REC reference: AC-2018-3156). Patients P9–P11 were consented and enrolled to the MYOGENE project, approved by the Institute of Genetics and Molecular and Cellular Biology IRB (DC-2012-1693). Tissue (DNA and skin fibroblasts) were obtained based on standard procedures. Muscle biopsies were obtained as part of the regular clinical diagnostic testing and were evaluated by standard light and electron microscopy protocols.

Molecular Genetic Analyses of Patients

Whole exome sequencing (WES) was performed in the 2 index patients (P1, P2) at the NIH Intramural Sequencing Center using the Illumina (San Diego, CA) TruSeq Exome Enrichment Kit and Illumina HiSeq 2500 sequencing instruments, and was combined with haplotype analysis in the entire family (as described¹³). Assuming autosomal recessive inheritance in a nonconsanguineous family, the haplotype data were analyzed to identify regions of shared haplotypes between the 2 affected siblings but not their unaffected siblings or parents. WES was performed in the 2 affected siblings (P1, P2) and analyzed for biallelic rare variants that were predicted to be damaging and shared between them. Given the highly specific-appearing clinical phenotype in the index family, an additional 6 patients (P3–P8) in 4 families were identified at neuromuscular centers in Europe and Asia. DNA was analyzed by direct Sanger sequencing of the candidate gene. In one additional family, *GGPS1* mutations were identified in 3 affected siblings (P9–P11) via WES, which was performed using the SureSelect Human All Exon 50 Mb capture library v5 (Agilent Technologies, Santa Clara, CA) and the Illumina HiSeq2500 platform. Sequence data were aligned to the GRCh37/hg19 reference genome, variants were annotated and filtered based on their frequency in Genome Aggregation Database (gnomAD; <http://gnomad.broadinstitute.org/>) and an in-house database containing >1,500 exomes, and the impact of the variants was predicted using SnpEff (<http://snpeff.sourceforge.net/>).

Histology and Immunohistochemical Staining

Muscle biopsies and skin biopsies were processed following standard procedures. Dermal fibroblasts derived from skin biopsies were cultured as described previously.¹⁴ Some of the dermal fibroblasts were converted to myoblasts with the Lenti-MyoD lentiviral system (Clontech Laboratories, Mountain View, CA). Cultured fibroblasts and muscle cryosections were processed with a standard immunohistochemical staining method.¹⁴ The following antibodies were used for immunohistochemical staining:

GGPS1 (N-term; Abcepta, San Diego, CA), desmin (clone DE-U-10; Sigma-Aldrich, St Louis, MO), LC3b (D11; Cell Signaling Technology, Beverly, MA), and ATP synthase beta (Thermo Fisher Scientific, Waltham, MA). Confocal images were captured with a Leica (Wetzlar, Germany) SP5 confocal laser scanning microscope.

GGPS Enzyme Activity Assay and Conformation Analysis

Wild-type and mutant GGPS identified in the patients were expressed in a bacterial expression system; enzyme activity was assayed using the substrates FPP and IPP as described previously.¹² The GGPS activities in Lenti-MyoD–converted myoblasts of normal controls and patients were also assayed as described before.¹⁵ The oligomerization of wild-type and mutant GGPS expressed in a bacterial system was measured by gel filtration chromatography using an ÄKTA Explorer as described previously.¹²

Generation of a *Ggps1* p.Y259C Knock-In Mouse

A knock-in mouse was generated under contract at genOway (Lyon, France) by insertion of a Y259C point mutation in exon 5a of the *Ggps1* gene (located 633bp downstream of the 5' end of exon 5a). The mutated *Ggps1* gene is expressed under the control of the endogenous *Ggps1* promoter. In addition, the *Ggps1* exon 4 is flanked by a validated FRT-neomycin-FRT-*loxP* cassette and by a single *loxP* site enabling the conditional deletion of the *Ggps1* gene. The FRT-neomycin-FRT-*loxP* cassette and the single *loxP* site are positioned as illustrated in the final figure.

Cell Membrane Repair Assay

Dermal fibroblasts derived from normal controls and Patient P6 were MyoD transfected using Lenti-MyoD, converted to myoblasts, and further differentiated into myotubes. These cells were tested in separate experiments for their cell membrane repair kinetics following focal pulsed laser injury in the presence of the cell impermeant dye FM 1-43 and following the dye intensity as described.¹⁶

Results

Clinical Phenotype

The index patient (P1; Fig 1) manifested symptoms prenatally with decreased fetal movements, and neonatally with a weak cry and a poor suck. By 12 months of age, she was diagnosed with bilateral sensorineural hearing loss (via brainstem auditory evoked response testing). She had delayed early motor milestones and walked independently at 18 months of age. She had intermittent episodes of diarrhea accompanied by poor feeding, muscle weakness, and elevated CK (up to 18,025U/l at 19 months of age). Progressive muscle weakness and contractures resulted in full-time wheelchair use by 11 years of age. She developed respiratory insufficiency, necessitating noninvasive ventilation, progressing to tracheostomy. Progressive scoliosis

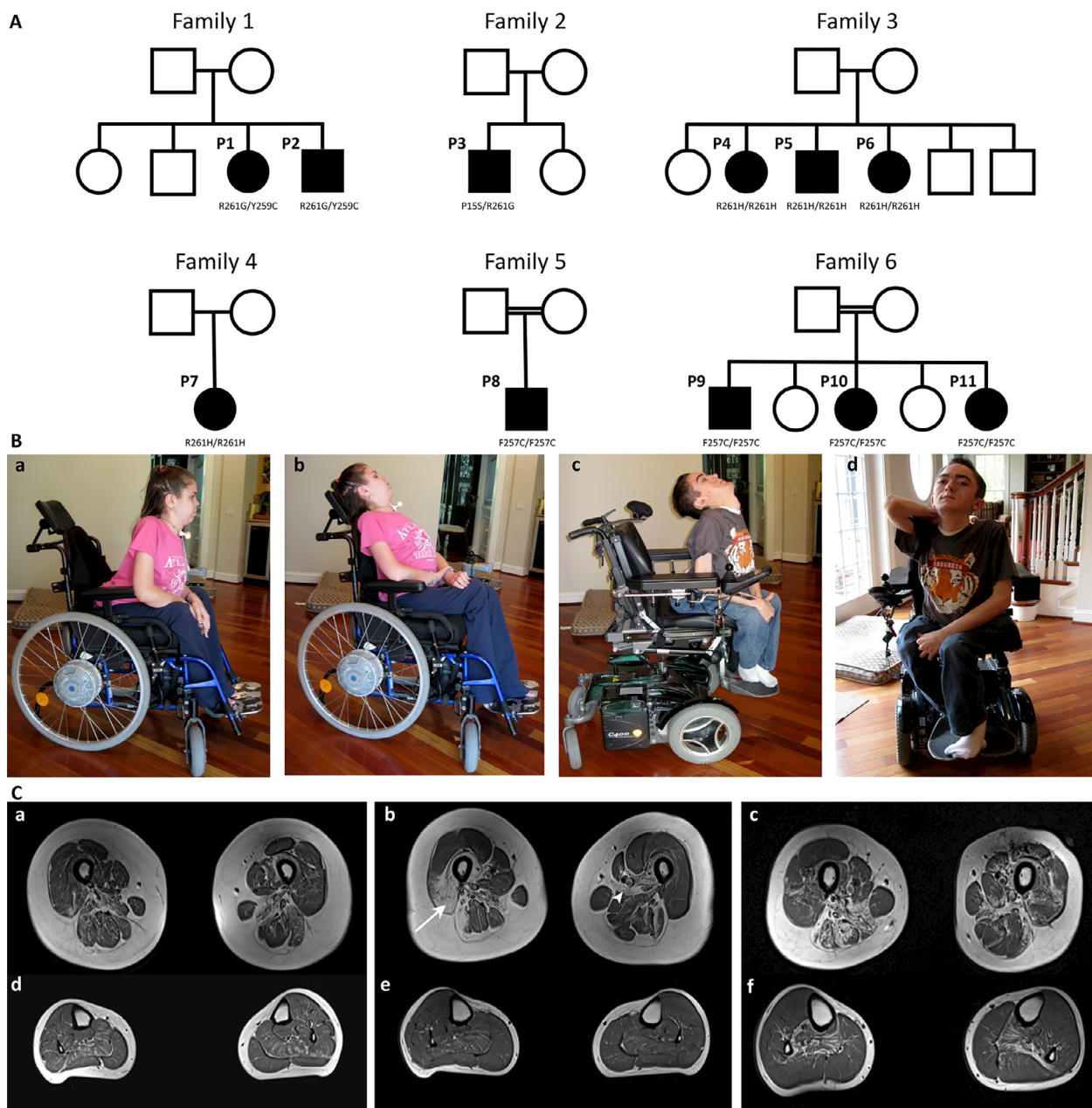


FIGURE 1: Autosomal recessive inheritance of *GGPS1* mutations and phenotypic characteristics of *GGPS1*-related muscular dystrophy. (A) Patient pedigrees demonstrating biallelic *GGPS1* mutations in 6 separate families. (B) Prominent lordosis (following spinal fixation surgery) and hip flexion, knee flexion, and elbow flexion contractures seen in patients P1 and P2, who both demonstrate diaphragm compressing maneuvers, including rocking back and forth or increasing intra-abdominal pressure on expiration by hand (a–d). P1 has a tracheostomy for ventilation (a and b), whereas P2 uses noninvasive ventilation in the form of bilevel positive airway pressure. Severe neck extension contracture is evident in P2 (c), necessitating support of the neck with the hand to promote upright head posture (d). (C) Muscle magnetic resonance imaging (MRI) findings in *GGPS1*-related muscular dystrophy. Muscle MRI performed in Family 3 (Patients P6 [a and d], P4 [b and e], and P5 [c and f]) shows variably increased T1 signal in muscles, indicative of fatty infiltration. There is evidence of relative sparing of the rectus femoris, sartorius, and gracilis muscles (a, b, and c) and relative involvement of the soleus muscle (d, e, and f). There is evidence of considerably asymmetric involvement with abnormal T1 signal in the lateral aspect of the vastus lateralis in Patient P4 on the right only (b, arrow) and abnormal T1 signal of the adductor longus on the left only (arrowhead). Patient 5 (c) has asymmetric involvement of the hamstrings with notable involvement of the hamstrings in the right leg and relative sparing of the hamstrings in the left leg.

necessitated spinal fusion at age 11 years. At 14 years of age, she had a gastrostomy tube placed for failure to thrive. She had amenorrhea, and following an endocrinologic evaluation was diagnosed with primary ovarian insufficiency. The index

patient's younger brother (P2) presented with a similar phenotype (Table), with congenital sensorineural hearing loss, muscular dystrophy with intermittent high elevations in CK (up to 11,250 U/l), respiratory insufficiency, and scoliosis.

TABLE. Xxx

	Family 1		Family 2	Family 3			Family 4		Family 5	Family 6		
Patient Identifier	P1	P2	P3	P4	P5	P6	P7	P8	P9	P10	P11	
GGPS1 mutations	p.[Tyr259Cys; Arg261Gly] c.[860A > G; 865C > G]		p.[Pro15Ser; Arg261Gly] c.[127C > T; 865C > G]	Homozygous p.Arg261His c.866G > A			Homozygous p.Arg261His c.866G > A	Homozygous p.Phe257Cys c.854 T > G	Homozygous p.Phe257Cys c.854 T > G	Homozygous p.Phe257Cys c.854 T > G		
Sex	F	M	M	F	M	F	F	M	M	F	F	
Ethnicity	Irish, German, and Polish	Irish, German, and Polish	English	Moroccan			Chinese (Han)	Algerian	Moroccan			
Current age, yr	31	29	22	46	45	44	14	21	22	11	8	
Age at last evaluation, yr	28	26	21	44	42	43	14	14	18	7	4	
Sensorineural hearing loss	Y	Y	Y	Y	Y	Y	Y	Y	Y	N	Y	
Wheelchair dependence (age)	Y (10 yr)	Y (13 yr)	Y (15 yr)	N	N	N	N	NA	Y (12 yr)	Y (11 yr)	N	
Respiratory insufficiency	Y	Y	Y	Y	Y	Y	Y	NA	Y	N	N	
FVC, % predicted	NA	NA	NA	74%	67%	79%	47%	NA	NA	NA	NA	
Scoliosis	Y	Y	Y	N	N	N	N	NA	Y	N	N	
Maximal recorded CK, U/l	18,025	11,250	6,641	336	4,900	281	14,143	1,600	3,633	NA	NA	
Primary ovarian failure	Y	—	—	Y	—	Y	Uncertain due to age	—	—	Uncertain due to age	Uncertain due to age	
Failure to thrive	Y	Y	Y	N	Y	N	Y	NA	Y	Y	Y	

CK = creatine kinase; F = female; FVC = forced vital capacity; M = male; N = no; NA = not available; Y = yes.

His fertility remains unknown, and he has not undergone a formal endocrinologic evaluation.

A further 9 patients in 5 families with recessively inherited mutations in *GGPS1* were subsequently identified, using direct *GGPS1* sequencing based on a suggestive phenotype (Patients P3–P8) or analysis of WES results (Patients P9–P11; see Table). Patient P3 was born prematurely (29 weeks gestational age) and was diagnosed with congenital sensorineural hearing loss. He carries compound heterozygous mutations in *GGPS1* (R261G; P15S) and has a phenotype most similar to P1 and P2, with whom he shares the R261G mutation. Like Patients P1 and P2, Patient P3 has had variably elevated CK values (up to 6,641 U/l) and has developed respiratory insufficiency, wheelchair dependence, scoliosis, and failure to thrive. In Family 3, 3 of 6 children are affected and carry homozygous R261H mutations in *GGPS1*, manifesting with a milder motor phenotype in that they all have muscle weakness but achieved the ability for a slow run and have maintained independent ambulation into adulthood.

All have sensorineural hearing loss, and both affected females have been formally diagnosed with primary ovarian insufficiency. The male has not undergone a formal endocrinologic evaluation but has no offspring at 45 years of age. Patient P7 in Family 4 is also homozygous for the R261H mutation in *GGPS1* and also manifests a comparatively milder phenotype from a motor perspective. At 14½ years of age, she remains independently ambulatory. Patient P8 in Family 5 is homozygous for the F257C mutation in *GGPS1* and was diagnosed with congenital sensorineural hearing loss. At the time of his last assessment at 14 years of age, he remained independently ambulatory. In Family 6, 3 of 5 children (Patients P9–P11) were identified via WES to carry homozygous F257C mutations in *GGPS1*, resulting in a moderate-to-severe phenotype, with all 3 siblings manifesting muscle weakness and failure to thrive. The oldest sibling (a 22-year-old male) has been a full-time wheelchair user since the age of 12 years, and has respiratory insufficiency and scoliosis. Of the younger (female) siblings, the

11-year-old uses a wheelchair full-time, whereas the 8-year-old remains independently ambulatory.

Thus, progressive muscle weakness and joint contractures resulting in loss of independent ambulation, respiratory insufficiency necessitating ventilation dependence, and severe scoliosis were seen in Patients P1, P2, P3, and P9, whereas the other patients had a less severe progression of weakness. Sensorineural hearing loss was present in all but one patient in this cohort and was the first symptom identified in those patients with milder motor phenotypes. Given that the hearing loss was diagnosed in some patients in the neonatal period and in others during childhood, the onset is likely congenital, as diagnosis relies on a formal audiometric evaluation. Primary ovarian insufficiency, also known as premature ovarian failure, has been diagnosed in all postpubertal females in this cohort, as confirmed by menopausal levels of follicle-stimulating hormone (FSH) in the setting of a history of amenorrhea (P1, FSH: 88.2IU/l) or infertility (P4, FSH: 50.3IU/l; P6, FSH: 53.2IU/l). Eight patients had evidence of failure to thrive and/or short stature, potentially suggestive of further endocrinologic

involvement. Of note, no cardiac or cognitive involvement has been noted in this cohort.

Whole-body muscle magnetic resonance imaging was performed in Patients P4–P6 and demonstrates variable increase in T1 signal in select muscles, resulting from fatty infiltration and thus consistent with an underlying muscular dystrophy (see Fig 1C). It is notable that these 3 patients all demonstrated relative sparing of the rectus femoris, sartorius, and gracilis muscles. Clear asymmetry of muscle involvement and heterogeneously distributed abnormal T1 signal in the hamstrings were seen in Patients P5 and P6.

Muscle biopsies were performed in 9 patients (P1–P9). Histology was dystrophic, with evidence of degeneration and regeneration and internalized nuclei. There were occasional rimmed vacuoles; the oxidative stains had peripherally increased oxidative reactivity in some fibers and corelike regions in other fibers. Electron microscopy revealed ultrastructural evidence of enlarged but structurally normal mitochondria (P8) as well as evidence of excess autophagic material (P1 and P8; Fig 2). The CoQ₁₀ level in muscle was determined to be normal in Patient P1. Of note, Patient P3

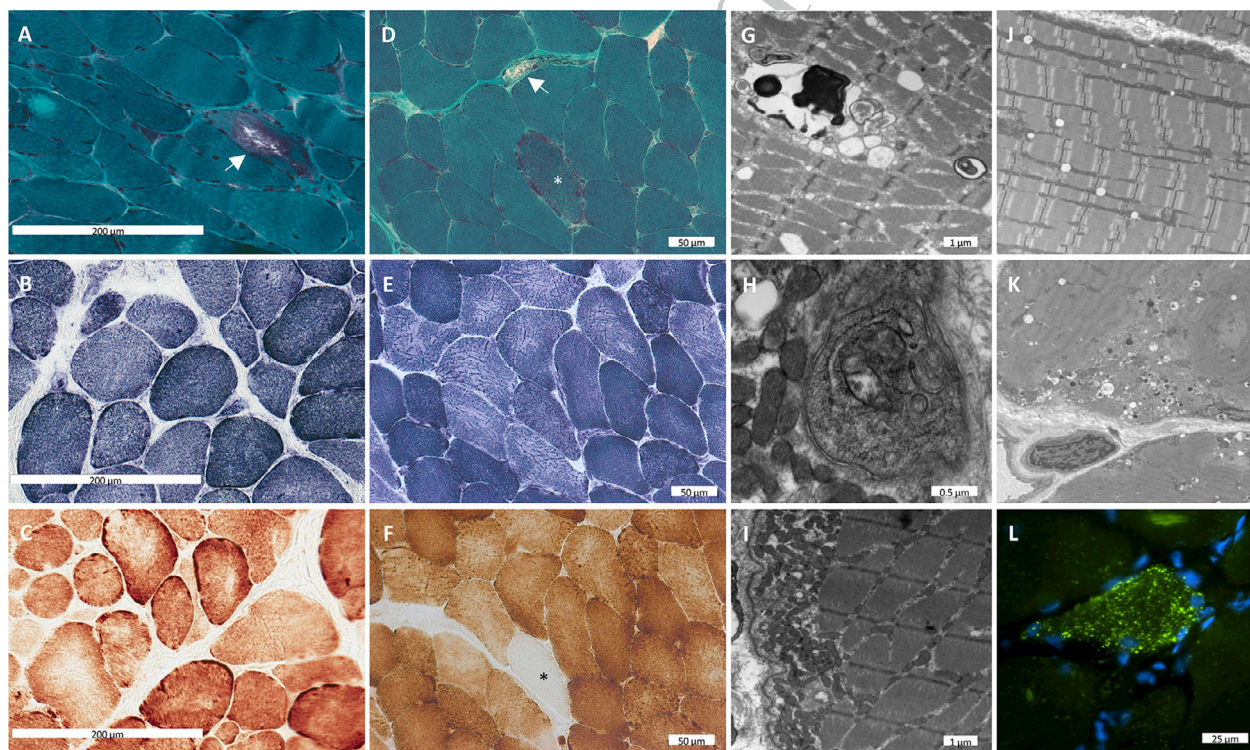
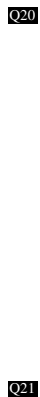


FIGURE 2: Histological, ultrastructural, and immunostaining characteristics of muscle in *GGP51*-related muscular dystrophy. (A–C) Muscle from a deltoid biopsy performed in Patient P1 at 21 years demonstrates nuclear internalization and a rimmed vacuole (arrow) on Gomori Trichrome staining (A). Nicotinamide adenine dinucleotide (NADH; B) and cyclooxygenase (COX; C) stains reveal focally irregular staining, including corelike regions (C). (D–F) Muscle from a deltoid biopsy performed in Patient P4 at 39 years demonstrates a ragged red fiber (asterisk) and myophagocytosis (arrow) on Gomori trichrome staining (D). NADH (E) and COX (F) staining demonstrate mildly irregular staining and a COX-negative fiber (asterisk; F). (G) Electron microscopy (EM) performed on P1's muscle biopsy reveals autophagic material including myeloid bodies. (H, I) EM of P2's deltoid biopsy at 19 years shows findings suggestive of mitophagy (H) and accumulation of subsarcolemmal mitochondria (I). (J–L) P8's quadriceps biopsy at 14 years reveals ultrastructural evidence of elongated mitochondria (J) and an accumulation of autophagic debris (K). Further evidence of disordered autophagy is seen by positive staining for the autophagy marker LC3B (L).



Q21

the symptoms are progressive in nature and can be severe. Muscle histological and ultrastructural findings are consistent with a dystrophic process with evidence of abnormal autophagy and mild mitochondrial changes.

In the index family, WES in the 2 index patients (P1 and P2) was combined with haplotype analysis on the entire

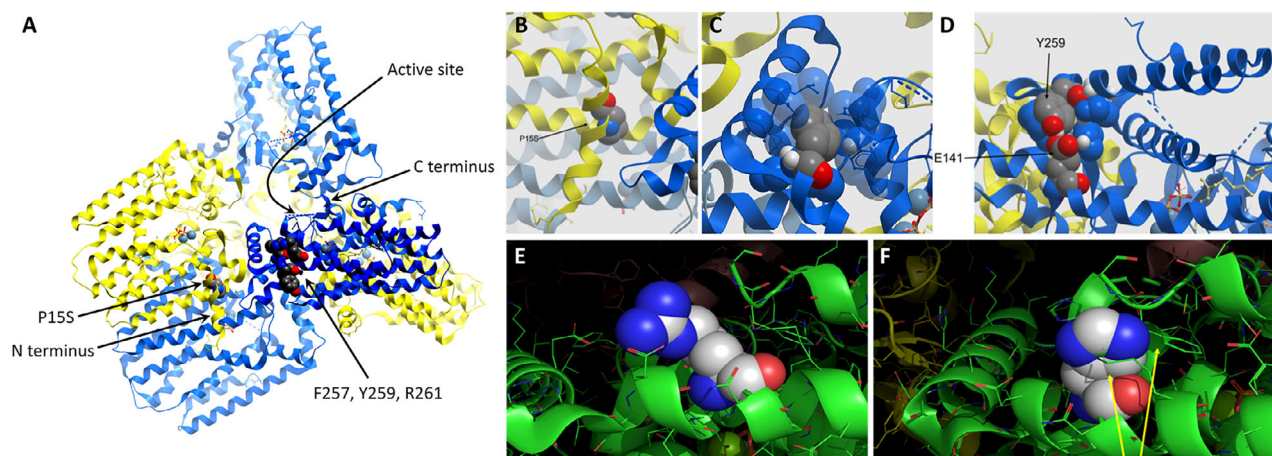


FIGURE 4: Geranylgeranyl diphosphate synthetase (GGPPS) modeling. (A) GGPPS hexamer overview showing the position of the mutations. Each dimer is composed of a blue and a yellow monomer; the whole molecule is made up of three dimers. F257, Y259, and R261 are shown on monomer A (blue); P15 is shown on monomer D (yellow). The C-terminus and active site of monomer A are arrowed. The N-terminus of monomer D is also annotated. Mutated residues at the C-terminus (F257, Y259, and R261) are located at an externally facing orientation of the 11th α -helix and outside of the barrel of the hexamer where the catalytic activity of GGPPS is located. The P15S mutation, on the other hand, maps to the first helical domain, which is in close interaction with residues 226–254 (region C in Fig 2A) of monomer A on the adjacent dimer, consistent with its purported role in assembly of the hexameric structure. (B–F) GGPPS mutant sites molecular model. Structural data were analyzed and figures were drawn using Molsoft Browser Pro and PyMOL 2. (B) P15 is inducing a kink in the helix. The side chain of the amino acid is in a relatively large pocket, which contains a water molecule (not shown). This area forms the interaction zone between monomers A (dark blue) and D (yellow) of dimers A/B and C/D. The mutant protein has a serine in this location. The side chain volume of serine is smaller than that of proline, and so modeling a serine residue here using PyMOL 2 shows no steric clashes. (C) F257 (gray balls) sits just buried below the surface of GGPPS. It is surrounded by mainly hydrophobic residues: Y180, H194, V248, and L251 (transparent blue balls). R261 (not shown) fills the gap above it. The van de Waals volume of phenylalanine is 135Å, so it is possible to substitute with the 86Å volume of cysteine, resulting in no steric hinderances. (D) Y259 sits on the surface with several interactions (F215, H219). The hydroxyl of Y259 sits closely with the oxygen (red) atoms of glutamic acid E141 and possibly forms an interaction. Replacing Y259 with C259 presents no steric clashes but probably abolishes any interaction with E141. (E) R261 sits on the outer surface of the GGPPS dimer facing the solvent. The side chain is shown as gray spheres for carbon atoms and blue for nitrogen, and the main chain is in green. (F) Modeling the replacement of this residue with a histidine highlights steric clashes with K265 and F294; however, K265 can rotate to minimize this clash. Replacing R261 with a glycine does not appear to cause a structural clash.

family, which ruled out 97.3% of the exome, leaving 2.07% consistent with recessive compound heterozygous inheritance. The compatible region was distributed on 3 separate regions on chromosome 1, and 1 region on chromosome 3, covering 55,538,583bp and containing 745 genes. Subsequently, WES data in P1 and P2 were analyzed for shared biallelic rare variants that were predicted to be damaging. Two variants (p.Y259C and p.R261G) in the geranylgeranyl diphosphate synthase 1 or *GGPS1* gene located in one of the compatible regions on chromosome 1 were identified as the only likely candidates to be responsible for the phenotype in this family. Both were extremely rare, p.Y259C was not present in gnomAD (<https://www.biorxiv.org/content/10.1101/531210v3>), whereas p.R261G was listed once, and both were predicted to be damaging (PolyPhen-2 prediction score of 1.000 and 0.711 for p.Y259C and p.R261G, respectively). Mutation and segregation in the family were confirmed by Sanger sequencing.

Given the highly specific-appearing clinical phenotype in the index family, an additional 6 patients in

4 families were identified at neuromuscular centers in Europe and Asia and analyzed by direct sequencing of *GGPS1*. One additional family (Family 6) with 3 affected siblings was identified by WES. In all patients, we identified biallelic pathogenic variants in *GGPS1*; 4 families were found to be homozygous, and in the remaining family compound heterozygous variants were identified. In all families, missense variants were identified: F257C (2 families), R261H (2 families), and R261G in compound heterozygosity with P15S in Family 2 (P3) and Y259C in Family 1 (P1 and P2). Allele frequencies (AFs) as determined in gnomAD were very low: P15S, AF = 0; F257C, AF = 0; Y259C, AF = 0; R261G, AF = 0.00003; R261H, AF = 0.00002. Rare heterozygous carriers for loss-of-function variants in *GGPS1* are listed in gnomAD and should therefore be asymptomatic. The pathogenic variants fell within a specific 5 amino acid region toward the C terminus around the start of helix 11, with as of yet unclear function (Fig 3A). In animals, geranylgeranyl diphosphate synthase is formed as a hexamer and in certain circumstances as an octamer, whereas in plants it is a

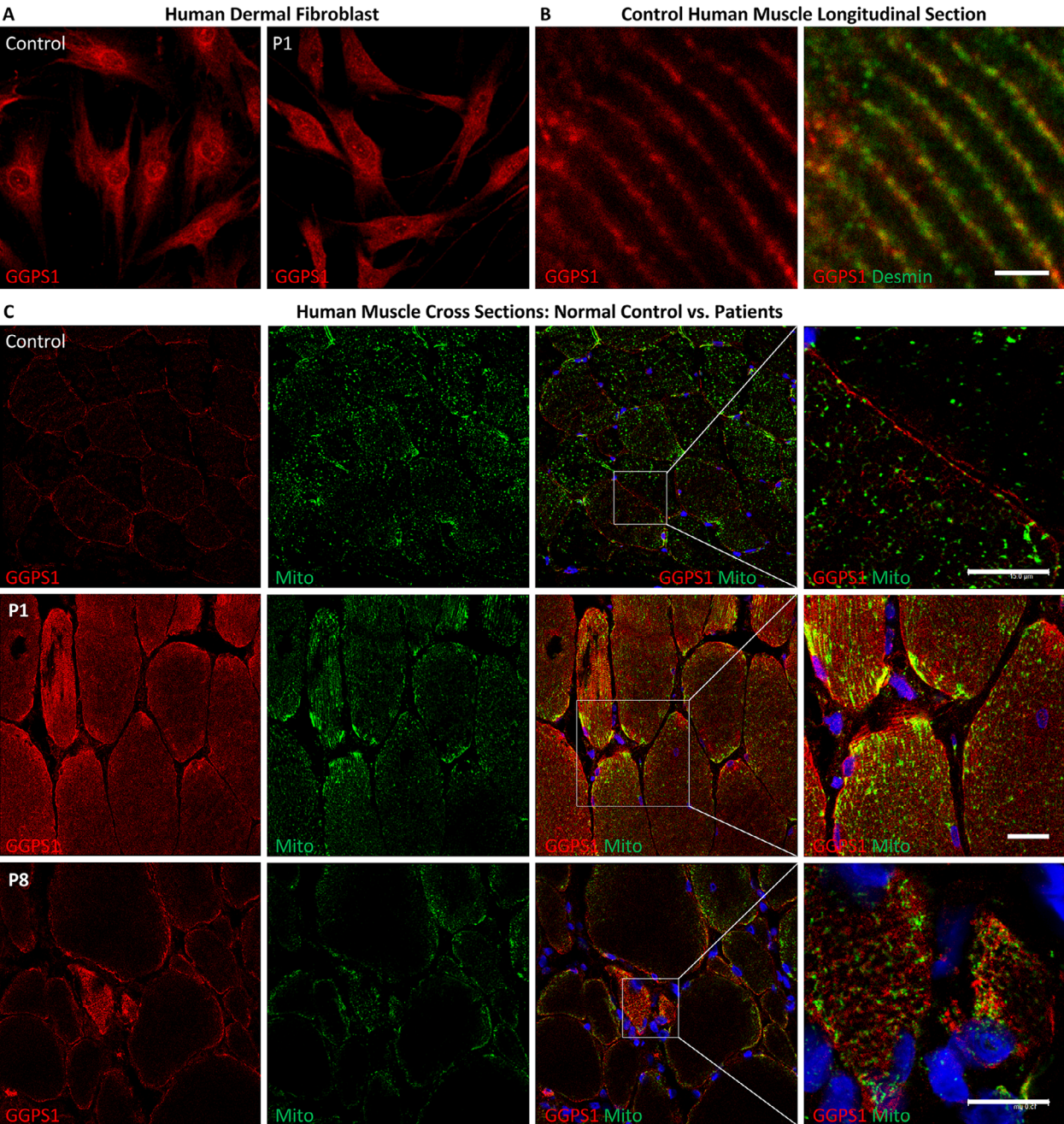


FIGURE 5: Geranylgeranyl diphosphate synthetase (GGPPS) in human dermal fibroblast and skeletal muscle. (A) In human dermal fibroblasts, GGPPS showed a rather uniform cytoplasmic expression, along with signals concentrated in some organelles and in the perinuclear region. No significant difference was observed between patient-derived fibroblasts (P1, with *GGPS1* compound heterozygous mutations: p.Y259C; R261G) and normal control fibroblasts. **(B)** GGPPS showed a prominent Z disc localization (Z disc labeled with desmin antibody) in the longitudinal section of normal human muscle biopsy. Scale bar = 2µm. **(C)** As shown in the human muscle cross section, an increased GGPPS immunoreactive signal was observed in the muscle of patients (P1 and P8) compared with normal control, with some focal, subsarcolemmal accumulation, which partially colocalizes with the mitochondrial marker adenosine triphosphate synthase beta. Scale bars = 15µm.

dimer.¹⁷ In silico modeling of GGPPS hexamer shows that this domain, in which all but one of the pathogenic variants (P15S) were clustered, is located toward the outside of the hexamer and not in the barrel where the catalytic core of the enzyme is located (Fig 4A). The first α -helix containing the P15S mutation is conserved and

involved in the formation of the trimer from the dimers (see Fig 3A). Whereas the catalytic domain itself is highly conserved across plants and animals, the mutated 5 amino acid domain is highly conserved in animals but not in plant *ggps1*, suggesting a function beyond the basic enzymatic activity of the enzyme in animal cells.

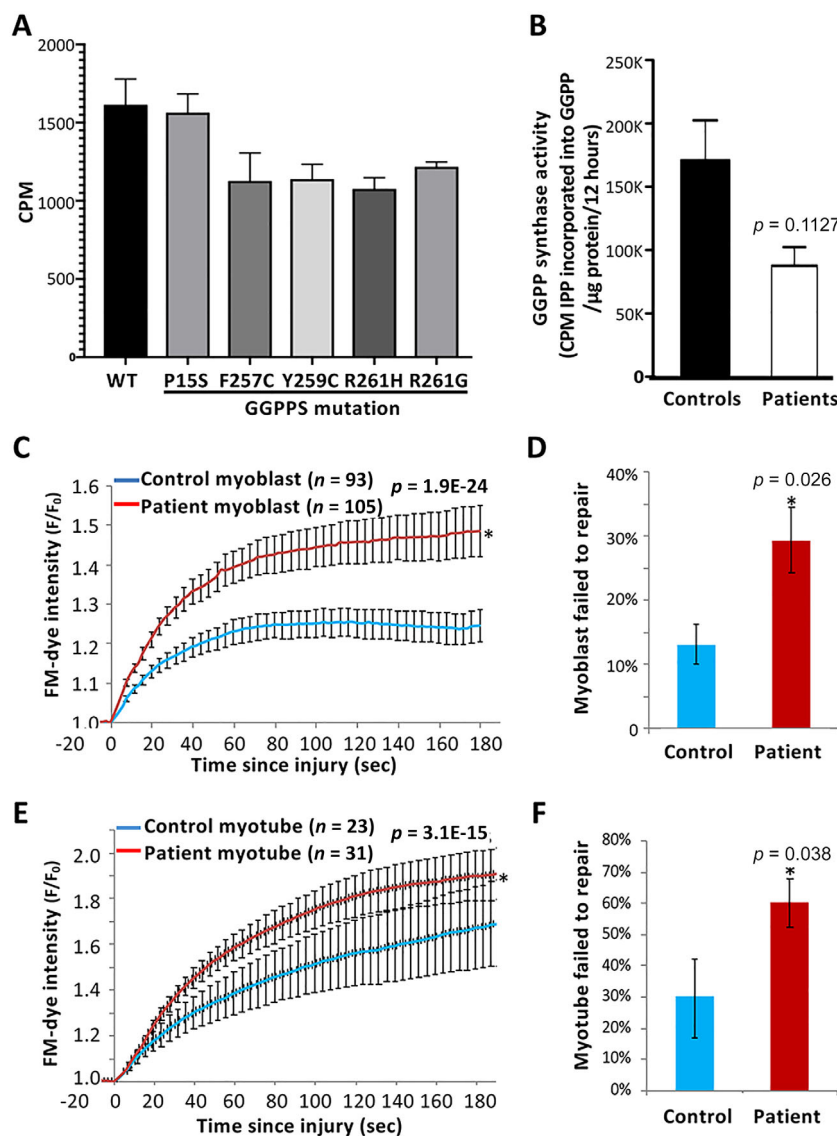


FIGURE 6: Geranylgeranyl diphosphate synthetase (GGPPS) enzyme activity and kinetics of human myoblast/myotube membrane repair following laser injury. (A, B) GGPPS catalytic enzyme activity (A) in wild-type (WT) and mutant GGPPS expressed in a bacterial expression system, using 10 μ M farnesyl-pyrophosphate/C14-isopentenyl pyrophosphate (IPP) as a substrate, showed the P15S mutant had similar activity as wild type; however, the other mutants (F259C, Y259C, R261G, and R261H) consistently showed reduced activity (range about 70–85% of wild-type activity; $n = 3$, technical repeats). (B) In human MyoD-converted myoblasts, the GGPPS enzymatic activity in pooled patients' cells (P1, P2, P6, and P8) decreased to about 50% of the activity in pooled control cells ($p = 0.1127$). (C–F) Patient myoblasts and myotubes have poor membrane repair ability. Patient myoblasts (C) and myotubes (E) were focally injured by laser, and the traces show the kinetics of the FM 1-43 dye fluorescence in patient myoblasts ($n = 93$) and control myoblasts ($n = 105$), indicating a delay in membrane repair in patient myoblasts (t test, $p = 1.9 \times 10^{-24}$). (D) Bar graph shows a greater fraction of the injured patient myoblasts failed to repair (30%) compared with control myoblasts (15%; t test, $p = 0.026$). (E) Similarly, differentiated myotubes showed significantly greater FM 1-43 dye entry in patient myotubes ($n = 23$) compared with control myotubes ($n = 31$; t test, $p = 3.1 \times 10^{-15}$). Again, a higher proportion of the injured patient myotubes failed to repair (60%) compared with normal control (30%; t test, $p = 0.038$). (F) Note that myotubes have less efficient repair at baseline compared to myoblasts, hence the difference to the mutant line, although still significant, is less obvious.

We were unable to generate a crystal structure of mutant GGPPS, while in silico modeling of the pathogenic variants did not result in major conformational or charge distribution changes of the 11th α -helix (see Fig 4B–D); only R261G results in the loss of a positive charge (see Fig 4E, F).

Immunohistochemical Analysis

In primary human dermal fibroblast, GGPPS immunocytochemistry revealed a rather uniform cytoplasmic expression consistent with its known cytosolic localization,¹⁸ along with signals concentrated at some organelles and the perinuclear region (Fig 5). There was no obvious difference in this pattern

in patients, as seen in P1 compared to controls. In longitudinal sections of control human muscle, GGPPS immunohistochemistry showed prominent localization to the Z disc, which was labeled with desmin. In patients, there was no deficiency of GGPPS immunoreactivity compared to controls; it appeared brighter and showed some focal, subsarcolemmal accumulation, partially colocalizing with the mitochondrial marker adenosine triphosphate (ATP) synthase beta.

Enzymatic Activity

We first measured enzyme activity of wild-type and mutant GGPPS expressed on bacteria. Using 10 μ M

FPP/IPP as a substrate showed that the P15S mutant had the same activity as wild type; however, the other mutants (F257C, Y259C, R261G, and R261H) consistently showed a reduced rate of activity of approximately 70 to 85% of wild type (Fig 6A). Activity assays performed with 20 μ M FPP/IPP in the presence of 20 μ M GGPP (thus a concentration of GGPP just below the concentration required for product inhibition in the wild-type enzyme) also had no effect on the enzyme activity in the mutants, suggesting that the mutations were not causing abnormal product release or an increase in their sensitivity to product inhibition (data not shown). Next, we measured GGPPS enzymatic activity in Lenti-MyoD-converted myoblasts of normal controls and patients (see Fig 6B). We found that enzymatic activity in samples pooled from 4 patients (P1, P2, P6, and P8) was decreased to about 50% of the activity in a pooled normal control sample.

GGPPS Conformation

GGPPS has been shown to be hexameric in structure as a trimer of dimers.¹⁵ The size of the enzyme produced in

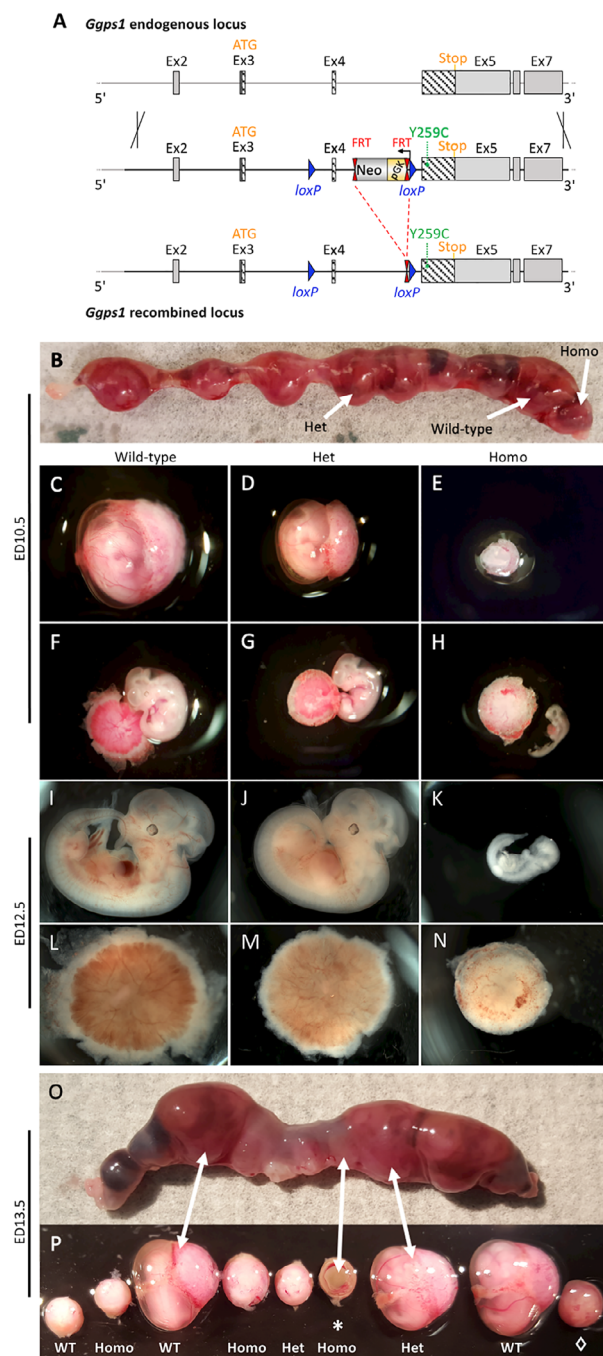


FIGURE 7: Generation of homozygous knock-in of Y259C mice results in delayed embryonic growth and embryonic lethality. (A) Schematic representation of the targeting strategy for creation of a knock-in Y259C mutant mouse. Hatched rectangles represent *Ggps1* coding sequences; gray rectangles indicate noncoding exon portions. The neomycin-positive selection cassette is driven by a phosphoglycerate kinase promoter (pGK) as indicated, and the *loxP* sites are represented by blue triangles and FRT sites by double red triangles. The initiation (ATG) and the Stop (Stop) codon used for isoform 3 where the Y259C mutation is present are indicated. *in vivo* Flp-mediated excision of the neomycin cassette is depicted. The diagram is not depicted to scale. (B) Photograph of a representative uterus from a heterozygous female at embryonic day (ED)10.5 following mating to a heterozygous male. Arrows indicate the embryos in C–E while in the uterus. (C–E) Photographs of embryos for each genotype enveloped by their yolk sac with placentas following dissection from the uterus. (F–H) Embryos and placentas isolated at ED10.5. Delayed growth in the homozygous knock-in embryos is shown in H. The knock-in embryo reflects the development typically observed at ED9.5 in wild-type (WT) mice. (I–K) Recovery of all genotypes at ED12.5 from heterozygous. Delayed embryonic growth in the homozygous embryo at ED12.5 (K) is reflective of the development of a WT embryo at ED10.5. (L–N) Placentas from the ED12.5 embryos above. The placenta from the homozygous knock-in embryo is reduced in size and is developmentally delayed compared to litter controls. (O) Photograph of a uterus from a heterozygous female at ED13.5 showing obvious differences in conceptus size. (P) Representative photograph of embryos in their yolk sac with placentas following dissection from the uterus for each genotype. A homozygous knock-in embryo in an advanced state of reabsorption is indicated with an asterisk. A WT and a heterozygous embryo are also observed to be undergoing reabsorption in this pregnancy. An embryo that we were unable to extract DNA from for genotyping is indicated with a diamond. Homo = homozygous; Het = heterozygous.

the bacterial expression system in solution was measured using gel filtration chromatography. We found that mutant enzymes eluted essentially at a similar point to the wild-type enzyme (see Fig 3C). The molecular weight of each mutant enzyme was in the expected range of 240 to 255kDa, suggesting the complexes are hexameric. There was a small amount of aggregated protein apparent for mutants Y259C, R261H, and R261G, which eluted with the void volume, but no indication of any smaller enzyme unit such as the dimer.

Cell Membrane Repair following Focal Injury

Patient fibroblasts were used to generate myoblasts, which were then differentiated into myotubes prior to testing the cell membrane repair kinetics and the ability of these cells to repair from focal laser injury as described.¹⁶ We observed greater dye entry, indicating a poor cell membrane repair, in both the patient myoblasts and myotubes as compared to the healthy controls (see Fig 6C, E traces). Consequently, there was about a 2-fold increase in the number of patient myoblasts that failed to repair (see Fig 6). Interestingly, despite the experimental challenge associated with the greater fragility of myotubes grown on a dish, which results in many more myotubes (compared to myoblasts) detaching upon injury, the patient myotubes demonstrated a 2-fold reduction in their ability to survive focal injury as compared to the control myotubes.

Ggps1 p.Y259C Knock-In Mouse

Given that total enzymatic activity was only moderately decreased in vitro, and that the identified mutations cluster in a very narrow, externally facing domain outside of the catalytic core of the enzyme, we surmised that the human disease-associated mutations would likely only interfere with a highly specific function or subcellular localization of the protein to explain the very specific clinical phenotype. As a total knock-out, the gene is not viable; we therefore created a knock-in mouse of the mutation p.Y259C (Fig 7A) detected in compound heterozygosity in the index family (Family 1) to study the effects of the mutant *GGPS1* on the organismal level. We chose this mutation, with the highest PolyPhen-2 score, to maximize our chances of detecting a phenotype in the mouse, as knock-in models of human missense mutations are frequently insufficiently penetrant. We were surprised to find that no litter included homozygous mutant animals. Timed pregnancies (see Fig 7B–P) revealed that homozygote Y259C knock-in embryos developed up to embryonic day (ED)12.5, with no live embryos observed after this point. No gross developmental abnormalities but a dramatically slowed rate of development was evident at

ED10.5, when homozygous Y259C knock-in embryos more closely resembled a wild type embryo at ED9.5, and at ED12.5 they resembled the typical development observed in wild-type embryos at ED10. Thus, detailed mechanistic studies relevant to the human phenotype were not possible in this mouse strain.

Discussion

There are 3 important clinical dimensions to this recognizable syndrome: muscular dystrophy, hearing loss, and infertility. The muscular dystrophy ranged from prenatal/congenital onset with progression to loss of ambulation and respiratory failure in early teenage years, to milder manifestations with preserved ambulation into adulthood (see Table). In P1, P2, and P7, there was a history of episodic worsening of weakness concomitant with higher CK elevations during episodes of diarrhea. Muscle magnetic resonance imaging performed in Family 3 (see Fig 1C) revealed variable evidence of fatty replacement of muscles consistent with a muscular dystrophy. The relative sparing of the rectus femoris, sartorius, and gracilis muscles and asymmetric involvement of muscles in this clinical context may be diagnostically helpful but can also be observed in other muscular dystrophies. Imaging of additional patients will be required to assess whether a consistent pattern will emerge. Muscle histology in 6 patients confirms degenerative features of muscular dystrophy but with ultrastructural findings of disordered autophagy and larger, but structurally normal-appearing, mitochondria, pointing to potential involvement of these organelles (see Fig 2).

To our knowledge, this triad of clinical findings has not been seen in another form of muscular disease. Notably, the sensorineural hearing loss (confirmed in all but one patient in this cohort) was congenital in onset, as it was apparent as a delay in early language acquisition or evident on the first formal audiometric testing performed. Primary ovarian insufficiency was present in all postpubertal females in this cohort, as confirmed by abnormally high FSH levels when evaluated for amenorrhea (P1) or infertility (P4 and P6). The manifestations of sensorineural hearing loss and primary ovarian insufficiency were not related to the severity of the muscular dystrophy. Although we were not able to obtain andrological examinations on the postpubertal male patients in our series, none of the 5 male adult patients has had children. Of interest, reduced expression of GGPPS in testis has been linked to infertility in men.^{19,20}

The sensorineural hearing loss observed in patients with *GGPS1*-related muscular dystrophy is most likely sensory organ-related and localized to the organ of Corti, consistent with cochlear implantation being highly

effective in all 4 patients in our cohort who underwent implantation. Hereditary sensorineural hearing loss is genetically and mechanistically very heterogeneous.^{21,22} None of the recognized forms of hereditary sensorineural hearing loss has muscular dystrophy associated as part of the phenotype. Hearing loss may occur in combination with a muscular dystrophy or a myopathy in early onset facioscapulohumeral dystrophy^{2,23} and Vici syndrome, a complex congenital multisystemic disorder caused by recessive mutations in autophagy regulator *EPG5* gene, which can also be associated with sensorineural hearing loss,^{24–27} as well with a vacuolar myopathy,²⁸ thus implicating abnormal autophagy regulation in the causation of sensorineural hearing loss and myopathy. Early onset sensorineural hearing loss and primary ovarian insufficiency without muscular dystrophy have been recognized in Perault syndrome, a syndrome that is genetically heterogeneous and associated thus far with mutations in the genes *HSD17B4*, *HARS2*, *LARS2*, *CLPP*, and *C10orf2*,³ implicating mitochondrial and peroxisomal pathogenesis in this constellation. Patients with mutations in the mitochondrial tRNA synthase genes *LARS2* or *KARS* in addition to sensorineural hearing loss and ovarian insufficiency may also have cerebral leukodystrophy.²⁹

Possible downstream effects of GGPPS dysfunction and thus GGPP deficiency would be predicted to include impaired geranylgeranylation of small GTPases of the Rab, and Rho/Rac families with consequences on organelles involved in autophagy (such as Rabs23/24/7b), mitochondrial fission and fusion (Rab32), and actin filament dynamics (RhoA/Rac/Cdc42). A defect in the geranylgeranyl prenylation would thus be an intuitive way to tie together some of the multisystemic effects seen in the patients, including in muscle. In support of impaired muscle cell membrane healing as contributing to the dystrophic process with its high CK, we were able to demonstrate significant delays in membrane healing in patient fibroblast MyoD-transformed myoblasts and myotubes. The defective membrane healing could point to deficits of membrane shuttling from late endosomal compartment to the membrane (such as Rabs11b/11/4) and/or of mitochondria to the site of injury.^{30,31} Some of the findings clinically (worsening of the weakness associated with diarrhea), histologically (occasional ragged red and cyclooxygenase deficiency fibers), and ultrastructurally (enlarged mitochondria) could also point to mitochondrial dysfunction as one of the involved mechanisms, at least for the muscle aspect of the disease in the more severe patients. In ongoing work, however, we have not yet been able to pinpoint a consistent change in the small GTPases or in the overall prenylome of the cells (not shown). Given the localization of the mutation, however, we

would speculate that the effects are more subtle and related to the required precise subcellular spatial and temporal resolution of GGPPS depending on the cellular state and needs.

Organism-wide complete inactivation of GGPPS function is not compatible with multicellular survival. A hypomorphic allele in *Drosophila* causes the *quemao* brittle hair phenotype.³² A complete knock-out of *Ggpps-1* in the mouse is not viable, so that a floxed allele of *Ggpps1* in the mouse has been generated,³³ allowing for several tissue-specific models to be created.^{19,34–38} Although not completely inactivating the enzyme, the resulting GGPPS deficiency state caused a plethora of abnormalities by disrupting the protein FPP/GGPP balance, resulting in both increased protein farnesylation (Rhe-b in cardiac myocyte, H-Ras in Sertoli cell, and Rhe-b in germ cell of testis) and decreased protein geranylgeranylation (K-Ras in lung epithelial cell, RhoA and Rab27 in oocyte, and RhoA in skeletal muscle cell). Interestingly, the MCK-Cre driving muscle-specific GGPPS inactivation did not cause abnormality in muscle fiber morphology, fiber type composition, running ability, or rotarod test but improved systemic insulin sensitivity by activating Irs-1/Pi3k/Akt pathway through decreasing RhoA geranylgeranylation. Because GGPPS enzyme activities of the mutant GGPPS identified in our patients were only mildly reduced, we speculate the function of these mutants may be different from general GGPPS activity reduction.

Interference with the mevalonate pathway has been linked to human disease (see Fig 3B). Pharmacological targeting of the mevalonate pathway includes the use of statins to block HMGCoA reductase, which can lead to the development of myopathy in a subset of patients.³⁹ Abnormal geranylgeranylation specifically has been reported in muscle biopsies from patients with statin myopathy as well as in cellular models⁴⁰ with reduced prenylation of small GTPases including Rab and RhoA, and increased apoptosis.⁴¹ The anti-bone-resorptive drug class of bisphosphonates directly inhibit farnesyl diphosphate synthase or GGPPS. Loss of bone-resorptive activity and osteoclast apoptosis is due primarily to loss of geranylgeranylated small GTPases.⁴² In this context, it is of interest that a rare genetic variant in *GGPS1* (Asp188Tyr) has been linked to an increased fracture risk.^{10,11,43} When expressed in cells, the Asp188Tyr variant leads to reduced enzyme activity.¹² In our patients, there was no apparent bone phenotype; however, none of the patients has been treated with bisphosphonates, so that it remains unclear whether our patient cohort would react to the drug with higher sensitivity.

The specific biallelic mutations identified in this patient cohort were all extremely rare, recessively acting

Q28

Q29

missense mutations, 3 of which (R261H, R261G, and F257C) were recurrent in different ethnic populations. All mutations except for one allele (P15S in Patient P3) define a stretch of 5 amino acids in the 11th α -helix as a functionally important microdomain that is specific to animal GGPPS and not seen in the plant enzyme. The changes induced by the mutations are not structurally dramatic, but they likely change the hydrogen bonding network within the helix. The domain is clearly outside the catalytic site, which is located within the barrel formed by the 10 helices, but it faces outward, where it could potentially interact with as yet to be defined binding partners involved in the localization or shuttling enzyme (see Fig 4A). Only the P15S mutation is outside of the narrow 5 amino acid domain, but it occurs in compound heterozygosity with the R261G mutation in the original domain.⁴⁴ It is possible that P15S represents a hypomorphic allele acting in conjunction with the R261G missense in the commonly mutated microdomain.

Enzymatic activity of GGPPS in patient-derived fibroblasts was only moderately impaired, to about 50%, a degree of enzymatic dysfunction that in metabolic disease in general should not lead to a phenotype. Heterozygous loss-of-function alleles in *GGPS1* are listed in gnomAD in presumably normal individuals. It is thus likely that the effects of the mutations on GGPPS function are more subtle, for instance, by impairing the dynamic subcellular localization of the enzyme for cell-type-specific processes. It is notable that our effort to generate a knock-in mouse of one of the missense mutations was unexpectedly severe in that it caused embryonic lethality, the cause of which is not entirely clear, but strong evidence for a clear underdevelopment of the placental/embryonic vascular unit was evident. Small GTPases, including Rap1, Rho, and Rab GTPases, have previously been reported to regulate cell-cell junctions in various cell types and developmental stages,^{45,46} including for vascular and heart morphogenesis.^{45,47,48} Although not providing a suitable model for the human disease, the severity of the phenotype seen in the resulting Y259C knock-in mouse confirms the sensitivity of organisms to GGPPS dysfunction as well as the general pathogenicity of the missense mutation. To address this, we are generating a new mouse line that is heterozygous for the knock-in allele and a floxed allele for tissue-specific “unmasking” of the missense, as well as a knock-in line for a milder missense seen in homozygosity in some of the patients.

Biallelic, highly specific missense mutations in *GGPS1* in 11 patients from 6 independent families define a unique new syndrome of muscular dystrophy with associated congenital sensorineural hearing loss and primary ovarian insufficiency in females, while also highlighting

the mevalonate/isoprenoid pathway as a novel, albeit still incompletely explored, pathway for muscular dystrophy, hearing loss, and infertility. Because of the fundamental role GGPPS plays in cellular processes at all levels, it is likely that the effects of the mutations described here will be highly specific as to their cellular mechanisms in muscle, inner ear, and ovary. Shedding light on these new mechanisms and pathways might also open avenues for therapeutic intervention.

Acknowledgment

This study was supported by intramural funds from the NIH National Institute of Neurological Disorders and Stroke (grant to C.G.B.). J.E.D. is supported by National Institute for Health Research Oxford Biomedical Research Centre, Oxford, United Kingdom. J.L. and J.B. are supported by France Génomique (ANR-10-INBS-09) and Fondation Maladies Rares within the framework of the “Myocapture” sequencing project.

We thank the patients and their families for their generous participation in this study; and Dr P. Mohassel for his help in evaluating the patients.

Author Contributions

A.R.F., Y.Z., J.R., and C.G.B. contributed to the conception and design of the study; all authors contributed to the acquisition and analysis of data; A.R.F., Y.Z., J.E.D., J.R., N.R., S.Do., M.S., E.M., T.Mar., J.K.J., T.S., and C.G.B. contributed to drafting the text and preparing the figures.

Potential Conflicts of Interest

T.V. reports personal fees from DZHK, Antisense Therapeutics, Biophytis, Capricor, Italfarmaco, Santhera, Servier, Sarepta, Solid Biosciences, Dynacure, DiNAQOR, and Catabasis outside the submitted work.

References

- Mercuri E, Bonnemant CG, Muntoni F. Muscular dystrophies. *Lancet* 2019;394:2025–2038.
- Tawil R. Facioscapulohumeral muscular dystrophy. *Handb Clin Neurol* 2018;148:541–548.
- Demain LA, Urquhart JE, O’Sullivan J, et al. Expanding the genotypic spectrum of Perrault syndrome. *Clin Genet* 2017;91:302–312.
- Goldstein JL, Brown MS. Regulation of the mevalonate pathway. *Nature* 1990;343:425–430.
- Xu N, Shen N, Wang X, et al. Protein prenylation and human diseases: a balance of protein farnesylation and geranylgeranylation. *Sci China Life Sci* 2015;58:328–335.
- McTaggart SJ. Isoprenylated proteins. *Cell Mol Life Sci* 2006;63:255–267.

7. Taylor JS, Reid TS, Terry KL, et al. Structure of mammalian protein geranylgeranyltransferase type-I. *EMBO J* 2003;22:5963–5974.
8. Schumacher MM, Elsabrouty R, Seemann J, et al. The prenyltransferase UBIAD1 is the target of geranylgeraniol in degradation of HMG CoA reductase. *Elife* 2015;4. doi: 10.7554/eLife.05560.
9. Shidoji Y, Tabata Y. Unequivocal evidence for endogenous geranylgeranoic acid biosynthesized from mevalonate in mammalian cells. *J Lipid Res* 2019;60:579–593.
10. Roca-Ayats N, Balcells S, Garcia-Giralt N, et al. GGPS1 mutation and atypical femoral fractures with bisphosphonates. *N Engl J Med* 2017;376:1794–1795.
11. Nguyen HH, van de Laarschot DM, Verkerk A, et al. Genetic risk factors for atypical femoral fractures (AFFs): a systematic review. *JBM Plus* 2018;2:1–11.
12. Roca-Ayats N, Ng PY, Garcia-Giralt N, et al. Functional characterization of a GGPPS variant identified in atypical femoral fracture patients and delineation of the role of GGPPS in bone-relevant cell types. *J Bone Miner Res* 2018;33:2091–2098.
13. Gu F, Wu A, Gordon MG, et al. A suite of automated sequence analyses reduces the number of candidate deleterious variants and reveals a difference between probands and unaffected siblings. *Genet Med* 2019;21:1772–1780.
14. Mohassel P, Liewluck T, Hu Y, et al. Dominant collagen XII mutations cause a distal myopathy. *Ann Clin Transl Neurol* 2019;6:1980–1988.
15. Kavanagh KL, Dunford JE, Bunkoczi G, et al. The crystal structure of human geranylgeranyl pyrophosphate synthase reveals a novel hexameric arrangement and inhibitory product binding. *J Biol Chem* 2006;281:22004–22012.
16. Horn A, Van der Meulen JH, Defour A, et al. Mitochondrial redox signaling enables repair of injured skeletal muscle cells. *Sci Signal* 2017;10. pii: eaaj1978.
17. Matsumura Y, Kidokoro T, Miyagi Y, et al. The carboxyl-terminal region of the geranylgeranyl diphosphate synthase is indispensable for the stabilization of the region involved in substrate binding and catalysis. *J Biochem* 2007;142:533–537.
18. Ericsson J, Runquist M, Thelin A, et al. Distribution of prenyltransferases in rat tissues. Evidence for a cytosolic all-trans-geranylgeranyl diphosphate synthase. *J Biol Chem* 1993;268:832–838.
19. Wang XX, Ying P, Diao F, et al. Altered protein prenylation in Sertoli cells is associated with adult infertility resulting from childhood mumps infection. *J Exp Med* 2013;210:1559–1574.
20. Bae JW, Kim SH, Kim DH, et al. Ras-related proteins (Rab) are key proteins related to male fertility following a unique activation mechanism. *Reprod Biol* 2019;19:356–362.
21. Egilmez OK, Kalcioğlu MT. Genetics of nonsyndromic congenital hearing loss. *Scientifica (Cairo)* 2016;2016:7576064.
22. Duman D, Tekin M. Autosomal recessive nonsyndromic deafness genes: a review. *Front Biosci (Landmark Ed)*. 2012;17:2213–2236.
23. Lutz KL, Holte L, Kliethermes SA, et al. Clinical and genetic features of hearing loss in facioscapulohumeral muscular dystrophy. *Neurology* 2013;81:1374–1377.
24. McClelland V, Cullup T, Bodi I, et al. Vici syndrome associated with sensorineural hearing loss and evidence of neuromuscular involvement on muscle biopsy. *Am J Med Genet A* 2010;152A:741–747.
25. Finocchi A, Angelino G, Cantarutti N, et al. Immunodeficiency in Vici syndrome: a heterogeneous phenotype. *Am J Med Genet A* 2012;158A:434–439.
26. Ozkale M, Erol I, Gumus A, et al. Vici syndrome associated with sensorineural hearing loss and laryngomalacia. *Pediatr Neurol* 2012;47:375–378.
27. Byrne S, Dionisi-Vici C, Smith L, et al. Vici syndrome: a review. *Orphanet J Rare Dis* 2016;11:21.
28. Hedberg-Oldfors C, Darin N, Oldfors A. Muscle pathology in Vici syndrome—a case study with a novel mutation in EPG5 and a summary of the literature. *Neuromuscul Disord* 2017;27:771–776.
29. van der Knaap MS, Bugiani M, Mendes MI, et al. Biallelic variants in LARS2 and KARS cause deafness and (ovario) leukodystrophy. *Neurology* 2019;92:e1225–e1237.
30. Schwartz SL, Cao C, Pylypenko O, et al. Rab GTPases at a glance. *J Cell Sci* 2007;120(pt 22):3905–3910.
31. Horn A, Jaiswal JK. Cellular mechanisms and signals that coordinate plasma membrane repair. *Cell Mol Life Sci* 2018;75:3751–3770.
32. Lai C, McMahon R, Young C, et al. Quemao, a drosophila bristle locus, encodes geranylgeranyl pyrophosphate synthase. *Genetics* 1998;149:1051–1061.
33. Yu X, Shen N, Zhang ML, et al. Egr-1 decreases adipocyte insulin sensitivity by tilting PI3K/Akt and MAPK signal balance in mice. *EMBO J* 2011;30:3754–3765.
34. Xu N, Guan S, Chen Z, et al. The alteration of protein prenylation induces cardiomyocyte hypertrophy through Rheb-mTORC1 signaling and leads to chronic heart failure. *J Pathol* 2015;235:672–685.
35. Diao F, Jiang C, Wang XX, et al. Alteration of protein prenylation promotes spermatogonial differentiation and exhausts spermatogonial stem cells in newborn mice. *Sci Rep* 2016;6:28917.
36. Jiang C, Diao F, Sang YJ, et al. GGPP-mediated protein geranylgeranylation in oocyte is essential for the establishment of oocyte-granulosa cell communication and primary-secondary follicle transition in mouse ovary. *PLoS Genet* 2017;13:e1006535.
37. Tao W, Wu J, Xie BX, et al. Lipid-induced muscle insulin resistance is mediated by GGPPS via modulation of the RhoA/rho kinase signaling pathway. *J Biol Chem* 2015;290:20086–20097.
38. Jia WJ, Jiang S, Tang QL, et al. Geranylgeranyl diphosphate synthase modulates fetal lung branching morphogenesis possibly through controlling K-Ras prenylation. *Am J Pathol* 2016;186:1454–1465.
39. Mammen AL. Statin-associated autoimmune myopathy. *N Engl J Med* 2016;374:664–669.
40. Beltowski J, Wojcicka G, Jamroz-Wisniewska A. Adverse effects of statins—mechanisms and consequences. *Curr Drug Saf* 2009;4:209–228.
41. Turner RM, Pirmohamed M. Statin-related myotoxicity: a comprehensive review of pharmacokinetic pharmacogenomic and muscle components. *J Clin Med* 2019;9. pii: E22.
42. Rogers MJ. New insights into the molecular mechanisms of action of bisphosphonates. *Curr Pharm Des* 2003;9:2643–2658.
43. Peris P, Gonzalez-Roca E, Rodriguez-Garcia SC, et al. Incidence of mutations in the ALPL, GGPS1, and CYP1A1 genes in patients with atypical femoral fractures. *JBM Plus* 2019;3:29–36.
44. Chang TH, Guo RT, Ko TP, et al. Crystal structure of type-III geranylgeranyl pyrophosphate synthase from *Saccharomyces cerevisiae* and the mechanism of product chain length determination. *J Biol Chem* 2006;281:14991–15000.
45. Kooistra MR, Dube N, Bos JL. Rap1: a key regulator in cell-cell junction formation. *J Cell Sci* 2007;120:17–22.
46. Fukata M, Kaibuchi K. Rho-family GTPases in cadherin-mediated cell-cell adhesion. *Nat Rev Mol Cell Biol* 2001;2:887–897.
47. Leung C, Lu X, Liu M, Feng Q. Rac1 signaling is critical to cardiomyocyte polarity and embryonic heart development. *J Am Heart Assoc* 2014;3:e001271.
48. Abu-Issa R. Rac1 modulates cardiomyocyte adhesion during mouse embryonic development. *Biochem Biophys Res Commun* 2015;456:847–852.